Electron. Mater. Lett., Vol. 12, No. 3 (2016), pp. 383-387
DOI: 10.1007/s13391-016-5452-3

Improving Charge Transport of P3HT:PCBM Organic Solar Cell using MoO_3 Nanoparticles as an Interfacial Buffer Layer

Jae-Hyoung Kim,† Eung-Kyu Park,† Ji-Hwan Kim, Hyeong Jun Cho, Dong-Hoon Lee, and Yong-Sang Kim*

School of Electronic and Electrical Engineering, Sungkyunkwan University, Suwon 16419, Korea

(received date: 28 December 2015 / accepted date: 1 March 2016 / published date: 10 May 2016)

In this work, P3HT:PCBM based organic solar cells (OSCs) were fabricated. We investigated the protection of PEDOT:PSS from active layer using the solution processed molybdenum oxide nanoparticles layer (MoO_3 NPs, ≤100 nm). The device structure was ITO/ZnO/P3HT:PCBM/MoO_3/PEDOT:PSS/Ag. A thin film MoO_3 NPs was spin-coated and it acts as a hole transporting layer between the active layer and PEDOT:PSS. The MoO_3 NPs based device showed an improved short circuit current compared without MoO_3 NP layer. The pristine OSCs showed short circuit current density (J_{sc}) of 11.56 mA/cm^2 and PCE of 3.70% under AM 1.5G (100 mW/cm^2). MoO_3 NPs based device showed an increased PCE of 4.11% with J_{sc} of 12.74 mA/cm^2. MoO_3 NPs also decreased the charge recombination and resistance of the OSCs.

Keywords: organic solar cells, molybdenum oxide, hole transport layer, charge recombination

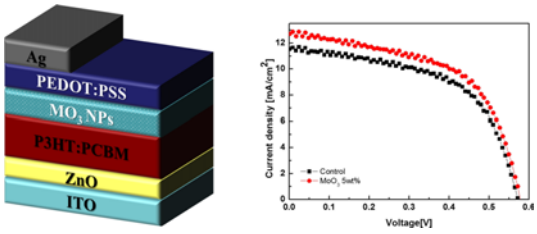

1. INTRODUCTION

Organic solar cells (OSCs) are of significant interest for light harvesting because of the potential for low cost of manufacturing large area through roll-to-roll coating technologies on flexible substrate.[1,2] Recently, significant efforts have been dedicated to the interface engineering of polymer solar cells.[3,4] The conducting conjugated polymer poly(3,4-ethylenedioxythiophene):poly(styrenesulfonate) (PEDOT:PSS) is a prominent material for the hole extraction layer. PEDOT:PSS exhibits a suitable work function value (~5.1 eV) for hole extraction. However, both the hygroscopic and acidic nature of PEDOT:PSS can result in the degradation of device performance.[5] One of the strategies to improve the efficiency of OSCs with given set of active materials is to insert an interfacial buffer layer between active layers and electrodes. The buffer layer can benefit OSCs cells by preventing undesired charge recombination[6] or keeping excitons away from electrodes.[7] The interface layer plays a significant role in improving the fill factor (F.F) by minimizing the contact resistance and charge recombination and enabling efficient extraction (or blocking) of hole and electrons. The transition metal oxides such as molybdenum oxide (MoO_3), silver oxide (Ag_xO), chromium oxide (Cr_2O_3), vanadium oxide (V_2O_5), nickel oxide (NiO_x), tungsten oxide (WO_3), and rhenium oxide (ReO_3) exhibit large work functions, and they are commonly applied as hole transport layer for the high efficiency collection of photogenerated charge carriers in inverted organic solar cells.[8-10] The MoO_3 NPs have various advantages on the efficiency of OSCs. Along with the increase of path length of the absorbed light, nanoparticles also enhances the structural stability of the layer leading to slower device degradation during prolonged illumination. NPs also block electron migration which reduces the charge recombination loss. The recombination mechanisms in polymer OSCs are not well established. However, numerous models have been reported discussing the charge recombination of OSCs.[11-14] Among them,

†J.-H. Kim and E.-K. Park contributed equally to this work
*Corresponding author: yongsang@skku.edu

molecular recombination has been proposed but has met with only limited success in explaining the current-voltage characteristics.[11] Also, Shockley-Read-Hall (SRH) recombination at interfacial traps was proposed as the dominant mechanism. In this study, we fabricated MoO_3 thin films based organic solar cells by spin coating method. The MoO_3 layer protected the P3HT:PCBM from PEDOT:PSS and improved charge recombination and resistance of organic solar cell. We also validated the role of metal oxide NPs in improving the electrical properties by analyzing the external quantum efficiency (EQE), charge collection probability and reduction in the recombination loss.

2. EXPERIMENTAL PROCEDURE

We fabricated the solar cells with the structure as shown in Fig. 1(a) (ITO/ZnO/P3HT:PCBM /PEDOT: PSS/Ag) and Fig. 1(b) (ITO/ZnO/P3HT:PCBM/MoO_3/ PEDOT:PSS/Ag). MoO_3 nanoparticles (Sigma Aldrich, ≤100 nm) were dispersed in isopropyl alcohol (IPA) with a concentration of 5 wt. %. Regioregular P3HT (Merck) and PCBM (Merck) were used as active layers without any further purification. The P3HT and PCBM (1:0.8 weight ratio) were dissolved in chlorobenzene and stirred at 90°C for 2 h. The ITO (15 Ω/square) coated glass substrate was cleaned in ultrasonic bath with acetone and isopropyl alcohol for 20 min each. The sol-gel zinc oxide (ZnO) precursor was deposited onto the ITO glass and annealed at 200°C for 20 min in air. Photoactive layer (P3HT:PCBM) solution was spin coated at 1200 rpm for 10 s to from 100 (±5) nm thick film. Its thickness was measured using surface profiler (alpha-step 500). Then MoO_3 film was deposited by spin-coating on the active layer. Finally, the PEDOT:PSS solution was spin coated on hexamethyldisilazane (HMDS) pre-coated surface of the MoO_3 NPs thin film. For the control device, in order to deposit hydrophilic PEDOT:PSS solution onto a hydrophobic active layer, PEDOT:PSS was mixed with 0.5 vol. % of Triton X-100 ($C_{14}H_{22}O(C_2H_4O)n$) nonionic surfactant. Thermal pre-annealing was conducted at 160°C for 10 min in a dry oven with nitrogen (N_2) ambient. The device was completed by thermal evaporation of 100 nm Ag cathode through a shadow mask defining an active area of 0.1 cm^2. Figure 1(c) show the energy band diagram of structures with MoO_3 NPs.

The current density versus voltage (*J-V*) characteristics were measured with *J-V* curve tracer (Eko MP-160) and solar simulator (Yamashita denso) under AM 1.5G (100 mW/cm^2) irradiation intensity. External quantum efficiency (EQE) spectra was measured under calibrated, monochromatic light illumination obtained from a xenon light source operating in the wavelength range of 400 - 700 nm (K3100, Mc Science). The light intensity was calibrated with a standard silicon cell (PV Measurements, Inc.). The output voltage of solar cell depends on the intensity of light. To study this dependency, we altered the illumination intensity of solar simulator, by varying the power of the lamp power supply. The intensity of the illumination was checked every time before the measurement with a calibrated silicon cell and meter. The surface morphology of the two different OSCs was studied using atomic force microscopy (AFM, Park System, XE-100). The entire fabrication and measurement processes were conducted in ambient air.

3. RESULTS AND DISCUSSION

The electrical properties of devices with MoO_3 NPs in buffer layer were characterized by means of electrochemical impedance spectroscopy (EIS), which is a powerful technique widely used to study interface charge transport process.[15] The measurement was performed in the dark, with electrical frequencies ranging from 100 Hz to 1 MHz.

Figure 2 shows EIS spectra of P3HT:PCBM solar cells based on pristine and with MoO_3 NPs thin film device. The high-frequency part of the spectra contain information of transport and series resistance elements, as well as dielectric contributions. The low frequency arc is attributed to recombination in the photoactive blend. Figure 2(a) and (b) show the frequency-dependent real and imaginary parts of impedance of the OSCs with MoO_3 NPs thin film. Figure 2(a) indicates the real part of impedance, where low frequency region (<100 Hz) and high frequency (>5000 Hz) can be seen. In the low frequency region, the real part of the

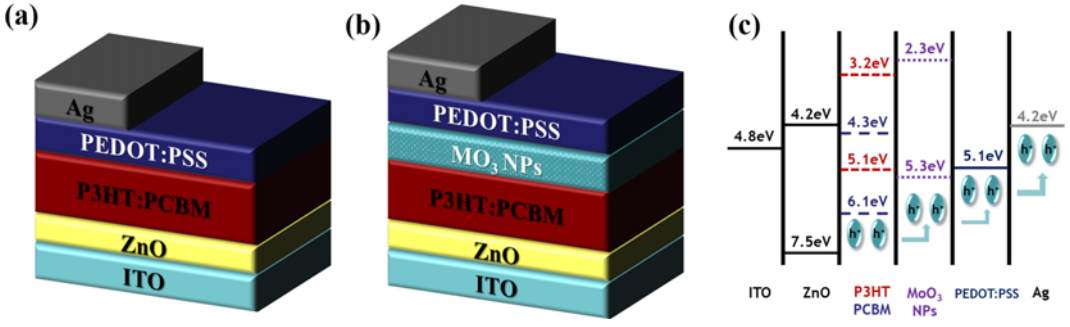

Fig. 1. The schematic of inverted organic solar cell (a) without MoO_3 NPs (b) with MoO_3 NPs. (b) Energy band diagram of the organic solar cells.

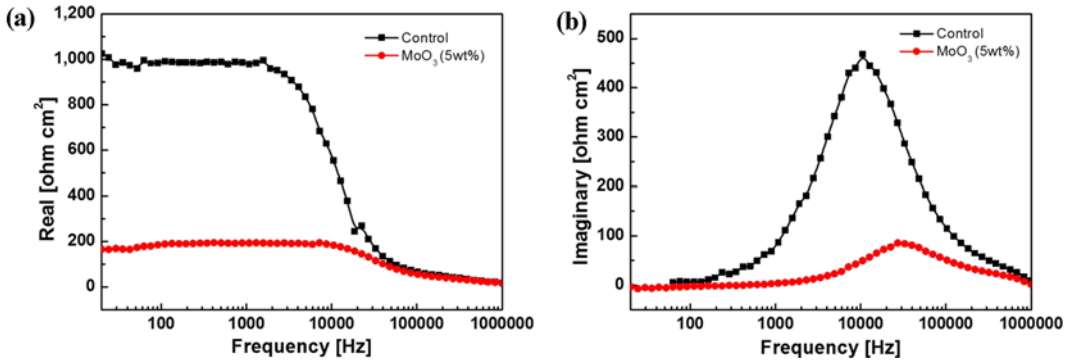

Fig. 2. (a) The frequency-dependent real parts and (b) the frequency-dependent imaginary parts of the impedance spectra for the devices with MoO_3 NPs thin film layer.

impedance is attributed to the series resistance (R_s) and in the high frequency region, the frequency-dependent real part of impedance corresponds to parasitic resistance (R_p). In MoO_3 NPs based device, R_p is smaller than control device, indicating a faster charge transport. Figure 2(b) shows the frequency-dependent imaginary parts of the impedance spectra, which is usually used to evaluate the relaxation frequency of the most resistive contribution. It can be seen that the characteristic frequency (f_{max}) centered at peak, shifts to high frequency with MoO_3 NPs thin film. The f_{max} indicated the characteristic relaxation time (τ). The value of τ can be defined by the relation $f_{max} \propto 1/\tau$. This small τ means efficient charge transport in the OSCs.[16,17] The constant phase element (CPE) is often used in place of a capacitance-like element to compensate for inhomogeneity in the interface, such as porosities, roughness, and surface states with CPE = 1/((CPE-T)(jw)^(CPE-P)) is defined by two values, CPE-T and CPE-P. If CPE-P equals 1, then the CPE is identical to an ideal capacitor without defects and/or grain boundary.[18,19] The parameters determined after the fitting of experimental data are summarized in Table 1.

As shown in Fig. 3, the P3HT:PCBM/PEDOT:PSS without

Table 1. EIS measurement of organic solar cells with MoO_3 NPs in interface layers.

	R_s [Ω cm^2]	R_p [Ω cm^2]	CPE-T [μF/cm^2]	CPE-P	f_{max} [kHz]
Control	18.9	1025	0.16	0.87	10.50
MoO_3 NPs	17.1	165	0.59	0.94	27.14

MoO_3 NPs has an RMS surface roughness of 1.43 nm and the OSC with MoO_3 NPs in interface layer has an RMS surface of 0.89 nm, respectively. The OSC without MoO_3 NPs film consequence in poor contact between the active layer and cathode and increases the resistance.

Figure 4(a) shows the log-log scale relationships of short circuit current density as function of light intensity. The charge collection probability is dependent on the incident light intensity. We measured the *J-V* characteristics the OSCs at different illumination intensities (20 to 130 mW/cm^2) without and with MoO_3 NPs thin film layer. Analysis of the recombination mechanism at short circuit is complicated by the simultaneous sweep-out during recombination. Because the sweep-out is approximately linear in intensity,

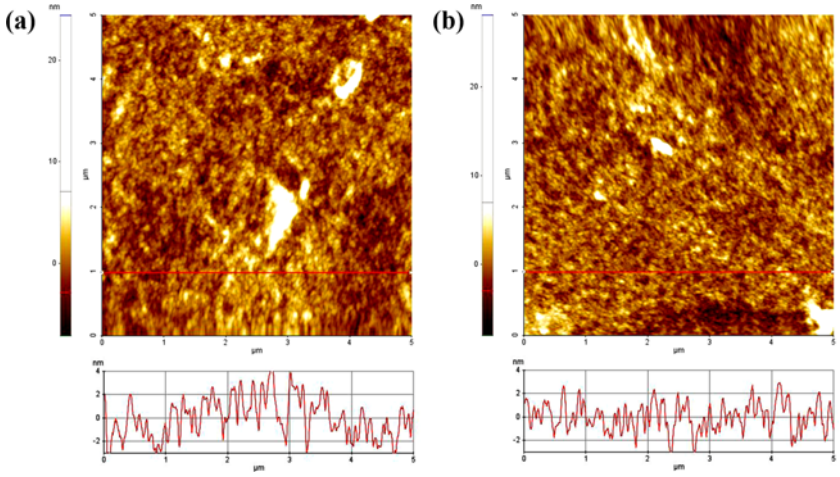

Fig. 3. AFM images of (a) P3HT:PCBM/PEDOT:PSS (b) P3HT:PCBM/MoO_3 NPs/PEDOT:PSS.

recombination shows up only as a small deviation from linearity.[20,21] The J_{sc} can be correlated to light intensity (I) by $J_{sc} \propto I^{\alpha}$ ($\alpha \leq 1$). At short circuit, the bimolecular recombination should be minimum ($\alpha \approx 1$) for maximum carrier sweep out. Any deviation from $\alpha \approx 1$ implies bimolecular recombination. The fitting of the data yield $\alpha =$ 0.977 which can be attributed to bimolecular recombination. With MoO_3 NPs thin film layer, $\alpha = 0.982$, which imply that bimolecular recombination is close to minimum.[20]

Figure 4(b) shows the semi log plot of dependence of open circuit voltage on the light intensity. The charge recombination studies at V_{oc} can provide detailed information on various mechanisms. The bimolecular recombination is the recombination of mobile electrons and holes at the interface of the donor/acceptor heterojunction.[21-23] For bimolecular recombination, the open circuit voltage is correlated to light intensity by $\Delta V_{oc} = (kT/e)\ \ln(I) + \text{constant}$. The k is the Boltzmann constant, T is the temperature, e is the electronic charge and I is the incident light intensity.

This implies that the slope of V_{oc} versus $\ln(I)$ is equal to kT/e for bimolecular recombination. The SRH recombination due to trap states can be clearly observed at low light intensities, where the cell's efficiency becomes highly dependent on the bias and light intensity (slope = 3.22 kT/e). The use of MoO_3 NPs thin film layer significantly reduces the trap assisted recombination with reduced slopes of 1.69 kT/e low light intensities.

Figure 5(a) shows the measured external quantum efficiency (EQE) of OSCs. A comparison of the increase in EQE between with and without MoO_3 NPs thin film device was performed. The device showed enhanced quantum efficiency in the broad wavelength range due to adequate absorption of light. Figure 5(b) shows the measured J-V characteristic under AM 1.5G (100mW/cm^2) irradiation intensity of OSCs with and without MoO_3 NPs. The control device showed a short circuit current density (J_{sc}) of 11.56 mA/cm^2. The device with MoO_3 NPs in buffer layer gave a J_{sc} of 12.74 mA/cm^2. Figure 1(c) shows the energy band diagram of MoO_3 NPs thin film based solar cells. The HOMO and LUMO of MoO_3 exists near polymer P3HT. This results in hole transfer from the PCBM to MoO_3 NPs and hole injections from MoO_3 NPs to the PEDOT:PSS. The improvement of J_{sc} as shown in Fig. 5(b) can be verified by the EQE results. The performance of the OSCs is summarized in Table 2.

As shown in Fig. 6, the performance of the OSC without MoO_3 interface layer decreased rapidly over 30 days, due to unprotected active layer. Contrarily, the device with MoO_3

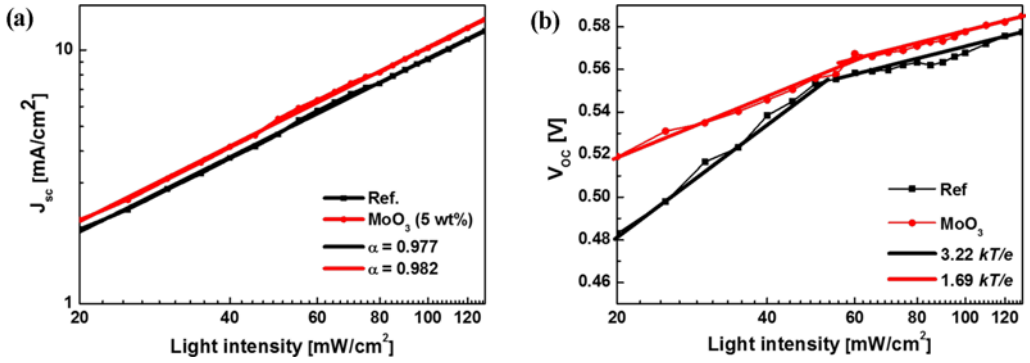

Fig. 4. (a) The measured J_{sc} of OSC with MoO_3 NPs plotted against light intensity (symbol) on the logarithmic scale and fitted with a power law (line) that yields α. (b) Measured V_{oc} of OSCs with MoO_3 NPs as a function of illumination intensity (symbol), together with linear fits of the data (solid lines).

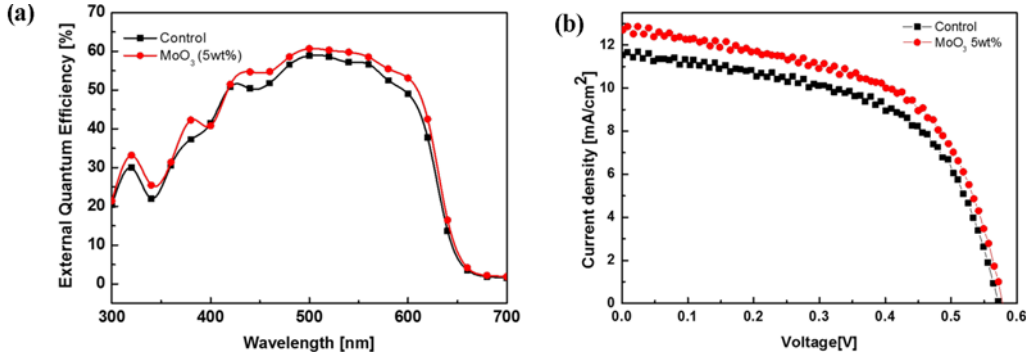

Fig. 5. External quantum efficiency characteristics of inverted organic solar cells with MoO_3 NPs (b) J-V characteristics of inverted organic solar cells using MoO_3 NPs under AM 1.5G irradiation at 100 mW/cm^2.

Table 2. Performance of organic solar cells with MoO_3 NPs.

	J_{sc} [mA/cm^2]	V_{oc} [V]	F.F	PCE [%]
Control	11.56	0.57	0.55	3.64
MoO_3 NPs	12.74	0.57	0.57	4.19

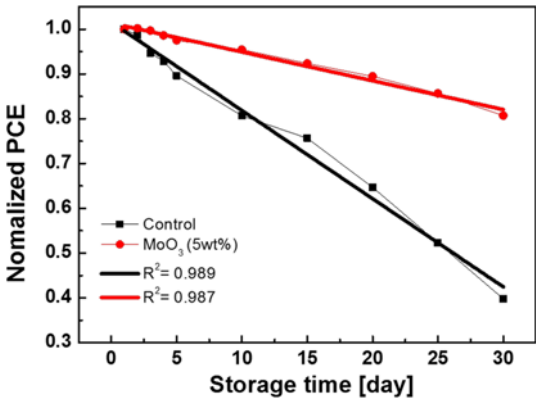

Fig. 6. Long-term stability of the PCE of OSCs with or without MoO_3 NPs in interface layer. The devices were stored in ambient air for 30 days.

layer showed high stability, even after storing in ambient air. After 30 days, the PCE of control device stored in ambient air dropped to about 38% of the initial PCE. However, the device with MoO_3 layer retained 80% of its initial PCE after 30 days. This result is in excellent agreement with the proposed theory. The presence of MoO_3 NPs protects the P3HT:PCBM from PEDOT:PSS and enhances the long-term stability of the OSCs.

4. CONCLUSIONS

The MoO_3 NPs, which can be dispersed in IPA solvent easily to form stable suspensions, has been demonstrated as a candidate to form an efficient anode buffer layer in an inverted organic solar cell. The devices based on P3HT: PCBM have achieved PCEs of 4.11% when MoO_3 NPs thin film act as the hole transport and active passivation layer. The solar cells with a pristine active layer showed a 3.70% efficiency, 3.22 (*kT/e*) monomolecular slope and 0.977 bimolecular while MoO_3 NPs layer based device showed a slope of 1.69 (*kT/e*), 0.982 recombination property under AM 1.5G illumination.

ACKNOWLEDGEMENTS

This work was supported under the framework of international cooperation program managed by National Research Foundation of Korea (No. 2014K2A2A2000803) and also supported by the Human Resources Development program (No. 20144030200580) of the Korea Institute of Energy Technology Evaluation and Planning (KETEP) grant funded by the Korea government Ministry of Trade, Industry and Energy.

REFERENCES

1. C.-H. Ji, I.-S. Oh, and S.-Y. Oh, *Electron. Mater. Lett*. **11**, 795 (2015).
2. J. Y. Kim, N. E. Coates, D. Moses, T. Nquyen, M. Dante, and A. J. Heeger, *Science* **317**, 222 (2007).
3. A. J. Heeger, *Adv. Mater.* **26**, 10 (2014).
4. P.-H. Wang, H.-F. Lee, Y.-C. Huang, Y.-J. Jung, F.-L. Gong, and W.-Y. Huang, *Electron. Mater. Lett*. **10**, 767 (2014).
5. E. Voroshazi, B. Verreet, T. Aernouts, and P. Heremans, *Sol. Energy Mater. Sol. Cells* **95**, 1303 (2011).
6. S. Han, W. S. Shin, M. Seo, D. Gupta, S.-J. Moon, and S. Yoo, *Org. Electron*. **10**, 791 (2009)
7. M. D. Irwin, B. Buchholz, A. W. Hains, R. P. H. Chang, and T. J. Marks, *PNAS* **105**, 2783 (2008).
8. C. W. Chu, S. H. Li, C. W. Chen, V. Shrotriya, and Y. Yang, *Appl. Phys. Lett.* **87**, 193508 (2005).
9. V. Shrotriya, G. Li, Y. Yao, C. W. Chu, and Y. Yang, *Appl. Phys. Lett.* **88**, 073508 (2006).
10. T. Stubhan, N. Li, N. A. Luechinger, S. C. Halim, G. J. Matt and C. J. Brabec, *Adv. Energy. Mater.* **2**, 1433 (2012).
11. P. Kumar, S. C. Jain, V. Kumar, S. Chand, and R. P. Tandon, *J. Appl. Phys.* **105**, 104507 (2009).
12. R. A. Street, M. Schoendorf, A. Roy, and J. H. Lee, *Phys. Rev. B* **81**, 205307 (2010).
13. C. Groves and N. C. Greenham *Phys. Rev. B* **78**, 155205 (2008).
14. C. G. Shuttle, B. O'Regan, A. M. Ballantyne, J. Nelson, D. D. C. Bradley, and J. R. Durrant, *Phys. Rev. B* **78**, 113201 (2008).
15. I. Riedel, J. Parisi, V. Dyakonov, L. Lutsen, D. Vanderzande, and J. C. Hummelen, *Adv. Funct. Mater.* **14**, 38 (2004).
16. S. Yuan, Y. Zhang, W. Liu, and W. Zhang, *Electrochimica. Acta* **116**, 442 (2014).
17. H. Zhou, Y. Zhang, J. Seifte, S. D. Collins, C. Luo, G. C. Bazan, T. Q. Nguyen, and A. J. Heeger, *Adv. Mater.* **25**, 1646 (2013).
18. Y. Zhang, L. Li, S. Yuan, G. Li, and W. Zhang, *Electrochim. Acta* **109**, 221 (2013).
19. G. Perrier, R. D. Bettignies, S. Berson, N. Lemaitre, and S. Guillerez, *Sol. Energy Mater. Sol. Cells.* **101**, 210 (2012).
20. A. K. K. Kyaw, D. H. Wang, C. Luo, Y. Cao, T. Q. Nguyen, G. C. Bazan, and A. J. Heeger, *Adv. Energy Mater.* **4**, 1301469 (2014).
21. X. Gong, M. Tong, Y. Xia, W. Cai, J. S. Moon, Y. Cao, G. Yu, C. L. Shieh, B. Nilsson, and A. J. Heeger, *Science* **325**, 1665 (2009).
22. S. R. Cowan, A. Roy, and A. J. Heeger, *Phys. Rev. B* **82**, 245207 (2010).
23. L. J. A. Koster, V. D. Mihailetchi, R. Ramaker, and P. W. M. Blom, *Appl. Phys. Lett.* **86**, 123509 (2005).